J|A|C|S
ARTICLES
Published on Web 03/31/2007

DNA Metastability and Biological Regulation: Conformational Dynamics of Metastable Ω-DNA Bulge Loops

Jens Völker,[†] Horst H. Klump,[‡] and Kenneth J. Breslauer*[,†,§]

Contribution from the Department of Chemistry and Chemical Biology, Rutgers-The State University of New Jersey, 610 Taylor Road, Piscataway, New Jersey 08854, Department of Molecular and Cellular Biology, University of Cape Town, Privatebag, Rondebosch 7700, Republic of South Africa, and The Cancer Institute of New Jersey, New Brunswick, NJ 08901

Received January 12, 2007; E-mail: kjbdna@rci.rutgers.edu

Abstract: Dynamic interchange between DNA conformations, including metastable states, can be of importance to biological function. In this study, we use a combination of spectroscopic and calorimetric techniques to detect and characterize kinetically trapped, metastable states in strand exchange and strand displacement reactions for bulge loop DNA conformations, here referred to as Ω-DNAs. We show that such metastable, Ω-DNA bulge loop states can stably coexist below 50 °C, while rearranging irreversibly at elevated temperatures to thermodynamically more stable states. Such dynamic interchange between metastable and globally stable DNA conformational states can be of importance in biological regulatory mechanisms.

Introduction

The biologically functional conformational space of DNA is far more polymorphic than originally suggested by early fiber diffraction images[1−4] and X-ray crystallographic studies[5−7] (and references therein). Subsequently, it has been demonstrated that DNA is able to adopt a multitude of local and global non-B DNA conformations in a sequence- and environment-dependent manner.[8−13] Recently, we and others have suggested that dynamic interchange between DNA conformations, including those that are only metastable, may be of critical importance for biological function and biotechnological applications.[14−25] It also has been proposed that transiently populated DNA conformations might serve as viable drug targets.[21,26] In this regard, a host of genetic diseases and chromosomal instabilities have been traced to DNA domains with a propensity to adopt alternative conformations in vitro. Models designed to rationalize the mechanisms of such disease development frequently invoke the formation of metastable DNA conformations as critical intermediates in vivo.[27−33] While numerous thermodynamically stable, non-B-DNA structures have been studied in detail, relatively little is known about the dynamic processes that lead to the formation and disappearance of metastable conformations of DNA. To address this deficiency, we have initiated a program of study that uses a combination of spectroscopic and calori-

[†] Rutgers-The State University of New Jersey.
[‡] University of Cape Town.
[§] The Cancer Institute of New Jersey.

(1) Watson, J. D.; Crick, F. H. *Nature* **1953**, *171*, 737−738.
(2) Arnott, S. *Prog. Biophys. Mol. Biol.* **1970**, *21*, 265−319.
(3) Wilkins, M. H.; Stokes, A. R.; Wilson, H. R. *Nature* **1953**, *171*, 738−740.
(4) Franklin, S. E.; Gosling, R. G. *Nature* **1953**, *171*, 740−741.
(5) Wang, A. H.; Quigley, G. J.; Kolpak, F. J.; Crawford, J. L.; van Boom, J. H.; van der Marel, G.; Rich, A. *Nature* **1979**, *282*, 680−686.
(6) Wing, R.; Drew, H.; Takano, T.; Broka, C.; Tanaka, S.; Itakura, K.; Dickerson, R. E. *Nature* **1980**, *287*, 755−758.
(7) Saenger, W. *Principles of Nucleic Acid Structure*; Springer-Verlag: NewYork, 1984.
(8) Pennisi, E. *Science* **2006**, *312*, 1467−1468 and references therein.
(9) Bloomfield, V. A.; Crothers, D. M.; Tinoco, I. *Nucleic Acids: Structures, Properties, and Functions*; University Science Books: Sausalito, CA, 2000, and references therein.
(10) Sinden, R. R. *DNA Structure and Function*; Academic Press: San Diego, CA, 1994, and references therein.
(11) Wells, R. D.; Harvey, S. C. Unusual DNA Structures. In *Proceedings of the First Gulf Shores Symposium*, Gulf Shores State Park Resort, April 6−8, 1987; Springer-Verlag: New York, 1988, and references therein.
(12) Dickerson, R. E.; Ng, H.-L. *Proc. Natl. Acad. Sci. U.S.A.* **2001**, *98*, 6986−6988 and references therein.
(13) Dickerson, R. E. *Methods Enzymol.* **1992**, *211*, 67−111 and references therein.
(14) Völker, J.; Makube, N.; Plum, G. E.; Klump, H. H.; Breslauer, K. J. *Proc Natl. Acad. Sci. U.S.A.* **2002**, *99*, 14700−14705.
(15) Bacolla, A.; Wells, R. D. *J. Biol. Chem.* **2004**, *279*, 47411−47414.
(16) Bacolla, A.; Wojciechowska, M.; Kosmider, B.; Larson, J. E.; Wells, R. D. *DNA Repair (Amsterdam)* **2006**, *5*, 1161−1170.
(17) Wang, G.; Vasquez, K. M. *Mutat. Res.* **2006**, *598*, 103−119.
(18) Bichara, M.; Wagner, J.; Lambert, I. B. *Mutat. Res.* **2006**, *598*, 144−163.
(19) Pearson, C. E.; Sinden, R. R. *Biochemistry* **1996**, *35*, 5041−5053.
(20) Seenisamy, J.; Rezler, E. M.; Powell, T. J.; Tye, D.; Gokhale, V.; Joshi, C. S.; Siddiqui-Jain, A.; Hurley, L. H. *J. Am. Chem. Soc.* **2004**, *126*, 8702−8709.
(21) Siddiqui-Jain, A.; Grand, C. L.; Bearss, D. J.; Hurley, L. H. *Proc. Natl. Acad. Sci. U.S.A.* **2002**, *99*, 11593−11598.
(22) Seeman, N. C. *Trends Biochem. Sci.* **2005**, *30*, 119−125.
(23) Seeman, N. C. *Methods Mol. Biol.* **2005**, *303*, 143−166.
(24) Seelig, G.; Yurke, B.; Winfree, E. *J. Am. Chem. Soc.* **2006**, *128*, 12211−12220.
(25) Klump, H. H.; Chauhan, M.; Mills, M.; Lin, C. *Arch. Biochem. Biophys.* **2006**, *453*, 93−100.
(26) Ren, J.; Qu, X.; Dattagupta, N.; Chaires, J. B. *J. Am. Chem. Soc.* **2001**, *123*, 6742−6743.
(27) McMurray, C. T. *Proc. Natl. Acad. Sci. U.S.A.* **1999**, *96*, 1823−1825.
(28) Sinden, R. R. *Nature* **2001**, *411*, 757−758.
(29) Kovtun, I. V.; Goellner, G.; McMurray, C. T. *Biochem. Cell Biol.* **2001**, *79*, 325−336.
(30) Usdin, K.; Grabczyk, E. *Cell. Mol. Life Sci.* **2000**, *57*, 914−931 and references therein.
(31) Wells, R. D.; Dere, R.; Hebert, M. L.; Napierala, M.; Son, L. S. *Nucleic Acids Res.* **2005**, *33*, 3785−3798 and references therein.
(32) Wells, R. D.; Bacolla, A.; Bowater, R. P. *Results Probl. Cell Differ.* **1998**, *21*, 133−165.
(33) Bowater, R. P.; Wells, R. D. *Prog. Nucleic Acid Res. Mol. Biol.* **2001**, *66*, 159−202.

10.1021/ja070258q CCC: $37.00

Table 1. Oligonulceotide Sequences

Family	Name	Length	Sequence
	X(CAG)$_6$Y	40 mer	5'-CA CGA GCA CGC CAG CAG CAG CAG CAG CAG CAC ACC GAA GC-3'
CAG- Ω-DNA			X (CAG)$_6$ Y
	Y'X'	22 mer	5'-GC TTC GGT GTG GCG TGC TCG TG-3'
			Y' - X'
	Y'(CTG)$_6$X'	40 mer	5'-GC TTC GGT GTG CTG CTG CTG CTG CTG CTG GCG TGC TCG TG-3'
CTG- Ω-DNA			Y' (CTG)$_6$ X'
	XY	22 mer	5'-CA CGA GCA CGC CAC ACC GAA GC-3'
			X - Y

metric techniques to characterize the energetic landscape of DNA, particularly, DNA conformational switches between metastable and thermodynamically more stable states. Such transformations may be important in the modulation of biological function.

Metastable, Slipped DNA Structures and Dynamic Mutation

To probe the energetic landscape of one class of metastable DNA conformations, we designed an oligonucleotide model system based on slipped DNA structures. Such structures frequently are invoked as critical metastable intermediates in processes that lead to dynamic DNA mutations, including DNA expansion/contractions and/or chromosomal instability.[34−38] Dynamic DNA mutations often are traced to highly repetitive DNA domains, such as triplet repeat DNAs, which frequently are associated with the development of debilitating human diseases.[39,40] Within highly repetitive DNA sequences, slipped DNA structures are proposed to form transiently via out-of-register base pair formation between distal parts of the repeat sequence.[19,41−46] Such slippage can result in the formation of large single-stranded bulge loop structures. In such structures, not all potential base pairs are formed. As a result, slipped DNA structures in vivo represent metastable conformational states that only form because they are trapped in local energy minima separated from thermodynamically more stable states by significant activation barriers. It is hypothesized that such transiently formed, metastable structures are incorrectly recognized and processed by the cellular replication and repair machinery, causing dynamic mutation[30,31,35,43,47] (and references therein). Insight into the forces that stabilize such metastable, slipped DNA intermediates should enhance our understanding of the forces that control development of dynamic DNA mutations. Such insights more generally expand our understanding of the conformational space available to DNA.

Scheme 1

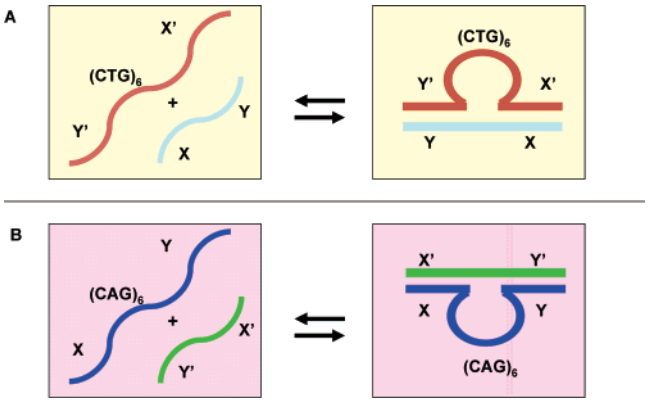

The Model System

We designed and synthesized two families of oligonucleotides, as shown in Table 1. These sequences can assemble into stable, bulge loop (Ω) structures through interactions between complementary domains within a 40mer [X(CAG)$_6$Y or Y′-(CTG)$_6$X′] and a 22mer (Y′X′ or XY), as shown in Scheme 1, panels A and B.

In this nomenclature, (see Table 1), the X′ and X domains, as well as the Y′ and Y domains are complementary. These complementary 11-base termini pair in the Watson−Crick sense, leaving the central, underlined 18-base domain of the 40mer strand looped out and unpaired, as shown in Scheme 1.

The 18-base bulge loop domains in both of these 40 + 22 constructs consist of (CNG)$_6$ triplet repeat sequences. Such bulge loop structures are suitable models for the metastable, transient, slipped DNA intermediates. We refer to these constructs as Omega DNA structures (Ω-DNA) because of their resemblance

(34) Pearson, C. E.; Nichol Edamura, K.; Cleary, J. D. *Nat. Rev. Genet.* **2005**, *6*, 729−742.
(35) Sinden, R. R.; Potaman, V. N.; Oussatcheva, E. A.; Pearson, C. E.; Lyubchenko, Y. L.; Shlyakhtenko, L. S. *J. Biosci.* **2002**, *27*, 53−65 and references therein.
(36) Pearson, C. E.; Sinden, R. R. *Curr. Opin. Struct. Biol.* **1998**, *8*, 321−330.
(37) La Spada, A. R.; Richards, R. I.; Wieringa, B. *Nat. Genet.* **2004**, *36*, 667−670.
(38) Richards, R. I. *Hum. Mol. Genet.* **2001**, *10*, 2187−2194.
(39) Richards, R. I.; Sutherland, G. R. *Cell* **1992**, *70*, 709−712.
(40) Sutherland, G.; Richards, R. *Proc. Natl. Acad. Sci. U.S.A.* **1995**, *92*, 3636−3641.
(41) Pearson, C. E.; Tam, M.; Wang, Y. H.; Montgomery, S. E.; Dar, A. C.; Cleary, J. D.; Nichol, K. *Nucleic Acids Res.* **2002**, *30*, 4534−4547.
(42) Pearson, C. E.; Wang, Y. H.; Griffith, J. D.; Sinden, R. R. *Nucleic Acids Res.* **1998**, *26*, 816−823.
(43) Panigrahi, G. B.; Lau, R.; Montgomery, S. E.; Leonard, M. R.; Pearson, C. E. *Nat. Struct. Mol. Biol.* **2005**, *12*, 654−662 and references therein.
(44) Tam, M.; Erin Montgomery, S.; Kekis, M.; Stollar, B. D.; Price, G. B.; Pearson, C. E. *J. Mol. Biol.* **2003**, *332*, 585−600.
(45) Khomyakova, E. B.; Petrova, M. V.; Minyat, E. E.; Ivanov, V. I. *FEBS Lett.* **1998**, *422*, 265−268.
(46) Minyat, E. E.; Khomyakova, E. B.; Petrova, M. V.; Zdobnov, E. M.; Ivanov, V. I. *J. Biomol. Struct. Dyn.* **1995**, *13*, 523−527.
(47) Kovtun, I. V.; Spiro, C.; McMurray, C. T. *Methods Mol. Biol.* **2004**, *277*, 309−319 and references therein.

Scheme 2

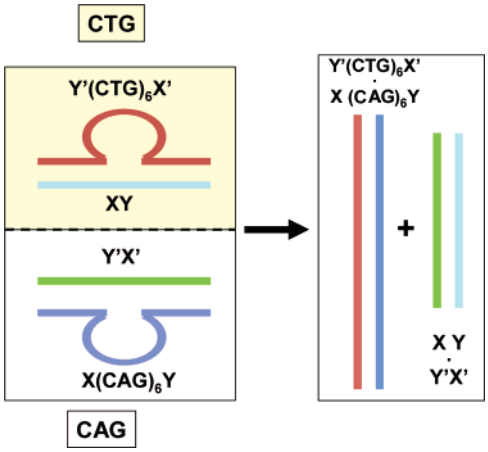

to the Greek letter Ω, when represented in two dimensions. We distinguish between the two Ω-DNAs according to the bases in the loop domain, e.g., CAG Ω-DNA and CTG Ω-DNA, respectively. We define these two 40 + 22 CNG Ω-DNA complexes as complementary since the sequence of the long strand (40mer) of one Ω-DNA is complementary to the sequence of the long strand (40mer) of the second Ω-DNA, while the sequences of the corresponding short strands (22mers) of each Ω-DNA complex are complementary to each other. As a result, the two Ω constructs can undergo strand exchange to form two Watson−Crick, fully paired duplexes, as shown in Scheme 2. These two Watson and Crick duplexes represent the thermodynamically more stable states relative to the two 40 + 22 bulge loop constructs.

We describe below the strand exchange behavior of these two 40mer Ω-DNA constructs when they are challenged with each other (Scheme 2), as well as the strand displacement reactions when they are challenged with either (1) a 40mer single strand that is fully complementary to the 5′, 3′, and loop domains of the Ω-DNA or (2) a competing 22mer single strand that is complementary only to the 5′ and 3′ domains of the Ω constructs. These strand displacement reactions are shown in Scheme 3.

We present and discuss the thermodynamic data and the associated energy landscapes and conformational dynamics of these systems. We also underscore the potential biological significance of such metastable, looped intermediates.

Materials and Methods

Materials. Oligonucleotides were synthesized by standard phosphoramidite chemistry using an Expedite DNA synthesizer, and were purified by repeated DMT on/DMT off reverse-phase HPLC as previously described.[14] Purified oligonucleotides where dialyzed against at least two changes of buffer containing NaCl, 10 mM cacodylic acid/Na-cacodylate, and 1 mM Na_2 EDTA to give a final concentration of 100 mM in Na^+ cations using dispo dialyzers with MWCO 500 Da. DNA extinction coefficients were determined by phosphate assay[48,49] in denaturing conditions (90 °C) and were found to be: $\epsilon_{\mathbf{X(CAG)6Y}(260nm,90°C)} = 368400\ M^{-1}\ cm^{-1}$; $\epsilon_{\mathbf{Y'(CTG)6X'}(260nm,90°C)} = 342900\ M^{-1}\ cm^{-1}$; $\epsilon_{\mathbf{XY}(260nm,90°C)} = 190400\ M^{-1}\ cm^{-1}$; $\epsilon_{\mathbf{Y'X'}\ (260nm,90°C)} = 186200\ M^{-1}\ cm^{-1}$.

UV Melting Studies. UV absorption versus temperature studies were conducted using a Aviv DS14 UV/vis spectrophotometer (Aviv Biomedical, Lakewood, NJ). Samples in 1 cm cells were heated from 0 °C to 99 °C in steps of 0.5 °C. At reaching the next set temperature, samples were equilibrated for 1 min before recording the absorption at 260 nm with a 5 s averaging time, resulting in a nominal heating rate of 0.1 °C/min. Oligonucleotide strand concentration was 1.5 μM.

CD Melting Studies. CD spectra as a function of temperature were recorded using an AVIV model 400 spectropolarimeter (Aviv Biomedical, Lakewood, NJ). Spectra were recorded in steps of 1 nm between 360 nm and 200 nm with an averaging time of 10 s using a 1 mm cell between 0 °C and 95 °C in 5 °C intervals. After subtraction of the relevant buffer scans, spectra were normalized for DNA concentration as described[50] and analyzed further. Oligonucleotide concentration was 10 μM in strand.

DSC Studies. DSC studies were conducted using a NanoDSCII differential scanning calorimeter (Calorimetry Science Corporation, Utah) with nominal cell volume 0.3 mL.[51] Oligonucleotides, at a concentration of 50 μM in strand, were repeatedly scanned between 0 °C and 100 °C with a constant heating rate of 1 °C/min while recording the excess power required to keep sample cell and reference cells at the same temperature. After conversion to heat capacity units and subtractions of buffer/buffer scans, the raw DSC traces were normalized for DNA concentration and analyzed using Origin software as previously described.[51−55] The calorimetric enthalpy (ΔH_{cal}) was derived by integration of the excess heat capacity curve, and ΔC_p was derived from the difference in the linearly extrapolated pre- and post-transition baselines at T_m. ΔS was derived by $\Delta H/T_m$, assuming "pseudo-monomolecular" behavior in which propagation dominates initiation. Although our constructs formally are bimolecular complexes, their concentration-dependent denaturation is not well described by a bimolecular process, as generally is the case for complexes of this size.[56] The theoretical entropy correction for a strictly bimolecular reaction of 21 cal mol^{-1} K^{-1} at $C_t = 50$ μM falls within the uncertainties of our entropy values, and is the same for all our constructs. As a result, inclusion of such a molecularity contribution simply scales the magnitudes, while not altering the relative differences in ΔS and ΔG between our constructs. ΔG at the reference temperature was calculated using standard equations taking into account the nonzero heat capacity changes, ΔC_p. The T_m is defined as the temperature at the midpoint of the integrated excess heat capacity curve for a given conformational transition. At this temperature, for a process that exhibits pseudo-monomolecular behavior, the sample is 50% denatured.

Results and Discussion

The Preformed, Metastable CNG Ω-DNA Complexes Coexist at Room Temperature. We measured the CD spectra and excess heat capacity curves of a 1:1 mixture of the two 40 + 22 bulge loop Ω-complexes and compared them to those expected for different numerical combinations of the experimental curves of the component states. Our results reveal that at room temperature the preformed Ω-DNA complexes stably coexist in solution without interacting (left side of Scheme 2) even though the competing 22mer and 40mer duplexes that could form via strand exchange correspond to the thermodynamically more stable states under our experimental conditions (right side of Scheme 2).

(48) Plum, G. E. In *Current Protocols in Nucleic Acid Chemistry*; John Wiley & Sons, Inc.: New York, 2000; pp 7.3.1−7.3.17.
(49) Snell, F. D.; Snell, C. T. *Colorimetric Methods of Analysis, Including Some Turbidimetric and Nephelometric Methods*; R. E. Krieger Pub. Co.: Huntington, N.Y., 1972.
(50) Cantor, C. R.; Schimmel, P. R. *Techniques for the Study of Biological Structure and Function*; W. H. Freeman: San Francisco, 1980.
(51) Privalov, G.; Kavina, V.; Freire, E.; Privalov, P. L. *Anal. Biochem.* **1995**, *232*, 79−85.
(52) Breslauer, K. J. In *Methods in Molecular Biology*; Agrawal, S., Ed.; Humana Press: Totowa, NJ, 1994; Vol. 26, pp 347−372.
(53) Breslauer, K. J. *Methods Enzymol.* **1995**, *259*, 221−242.
(54) Marky, L. A.; Breslauer, K. J. *Biopolymers* **1987**, *26*, 1601−1620.
(55) Privalov, P. L.; Potekhin, S. A. *Methods Enzymol.* **1986**, *131*, 4−51.
(56) Plum, G. E.; Grollman, A. P.; Johnson, F.; Breslauer, K. J. *Biochemistry* **1995**, *34*, 16148−16160.

Scheme 3

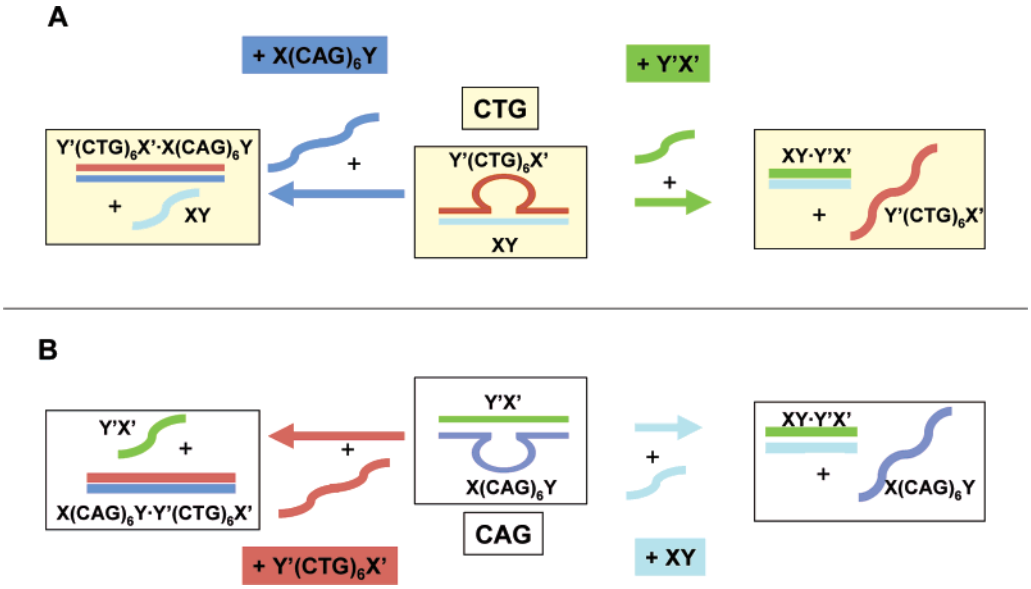

Thermally Induced Strand Exchange Occurs between the Two CNG Ω-DNA Complexes. Upon heating above a threshold temperature, the two CNG Ω-DNA complexes interact by swapping strands to form the thermodynamically more stable 22mer and 40mer duplex states (see Scheme 2). Once this exchange reaction takes place, the 40 + 22 bulge loop Ω-DNA complexes cannot reform from the Watson−Crick 40mer and 22mer duplexes; in other words, the temperature-induced strand exchange is irreversible. Thus, when combined at sufficiently low temperatures, the two bulge loop Ω-DNA duplexes represent a metastable system trapped within a local minimum. Upon heating beyond the thermal induction of the strand exchange, the newly formed 22mer and 40mer duplexes independently melt to their respective single-stranded states.

Assignment of the States and Their Transformations. CD Spectra. Prior to heating, the measured CD spectrum of the 1:1 mixture of the two 40 + 22 bulge loop Ω-DNA duplexes is the sum of the CD spectra of the individual Ω-DNA complexes. This spectrum differs significantly from that of the sum of the CD spectra of the 40mer and the 22mer Watson−Crick duplexes (Figure 1 panels I and II). Upon heating above 50 °C, however, a marked and irreversible change in the measured CD spectrum occurs. Upon cooling, the CD spectrum reflects the sum of the CD spectra of the two Watson−Crick, fully helical duplexes, rather than the sum of the spectra of two noninteracting Ω-DNAs (Figure 1, Panels I and III). These observations are consistent with the irreversible strand exchange process shown in Scheme 2.

DSC and UV Melting Profiles. The thermally induced change in the CD spectrum correlates with an unusual exothermic (negative) peak in the corresponding excess heat capacity curve (Figure 2, Panel II) and with an equally unusual thermally induced hypochromic transition in the optical melting curve at 260 nm (Figure 3). The exothermic (negative) peak in the heat capacity curve and the hypochromic transition in the optical melting curve are observed only during the initial heating of the 40 + 22 bulge loop Ω samples, being absent in all subsequent heating and cooling scans, consistent with an irreversible process.

An exothermic transition in the DSC profiles suggests formation of a more ordered structure, such as would be expected if the 40 + 22 Ω-DNA complexes converted to the corresponding 22mer and 40mer duplexes via strand exchange.[14] Similarly, the hypochromic change in Figure 3 likely reflects the increase in the number of base pairs and extended stacking interactions that result when the two 40 + 22 Ω-DNA complexes rearrange via strand exchange to form the 22mer duplex and 40mer duplex. In thermal scans subsequent to the exothermic/hypochromic transition observed in the initial melt, two conventional and reversible thermally induced endothermic/hyperchromic melting transitions are observed in the excess heat capacity and the optical melting curves of the 1:1 mixture of 40 + 22 Ω complexes. These transitions coincide exactly with the excess heat capacity and optical melting curves independently and directly measured for the isolated 22mer and 40mer duplexes (Figure 2, Panels II and III, and Figure 3). Neither the optical melting curve nor the calorimetric excess heat capacity curve can be modeled by the sum of the isolated, individual 40 + 22 Ω-DNA melting curves. In the aggregate, these observations are consistent with thermally induced strand exchange between the two bulge loop Ω-DNA constructs to form irreversibly the 40mer and 22mer fully paired Watson−Crick duplexes, as shown in Scheme 2.

In summary, at low temperature the two metastable Ω-DNA complexes stably coexist and do not interact. Once the sample is heated above the temperature of the exothermic reaction, strand exchange takes place, and the two helical duplexes form. The exothermic transition reflects the rearrangement/strand exchange between the two coexisting metastable states. Such an exothermic process only can be observed if a significant activation energy barrier has been overcome, which occurs upon heating. Once this activation barrier has been surmounted, the exchange process proceeds spontaneously to form the thermodynamically more stable, fully paired Watson−Crick duplexes.

The DSC and optical melting curves reveal that this irreversible strand exchange starts at temperatures below the melting transition of the individual Ω-DNAs. This observation makes it unlikely that the strand-swapping reaction proceeds via the

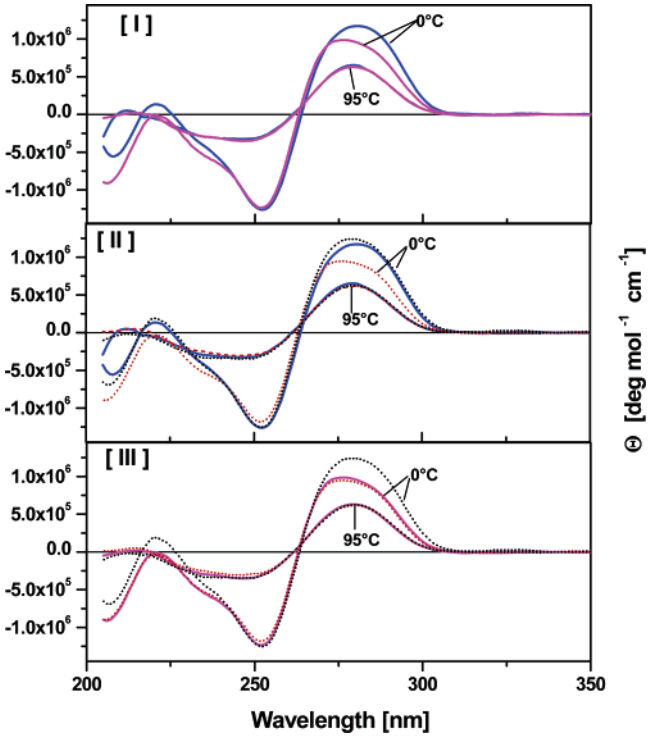

Figure 1. CD curves of the exchange reaction. (Panel I) Experimentally measured CD spectra of a 1:1 mixture of CAG Ω-DNA and CTG Ω-DNA at 0 °C, both prior to heating (blue) and after heating and cooling (magenta). (Panel II) Comparison of the measured CD spectrum (blue, solid) prior to heating with the CD spectra calculated for a 1:1 mixture of the CAG Ω-DNA and CTG Ω-DNAs (black stippled line), and calculated for the 1:1 mixture of the 22mer duplex and the 40mer duplex (red stippled line). (Panel III) Comparison of the corresponding experimental CD spectrum after heating (magenta) to the calculated spectra as noted for Panel II. Also shown as internal controls in Panels I, II, and III are the calculated (stippled red and black lines) and measured (solid blue and magenta lines) CD spectra at 95 °C. Calculated spectra are derived by summation of experimentally measured spectra of the isolated individual components.

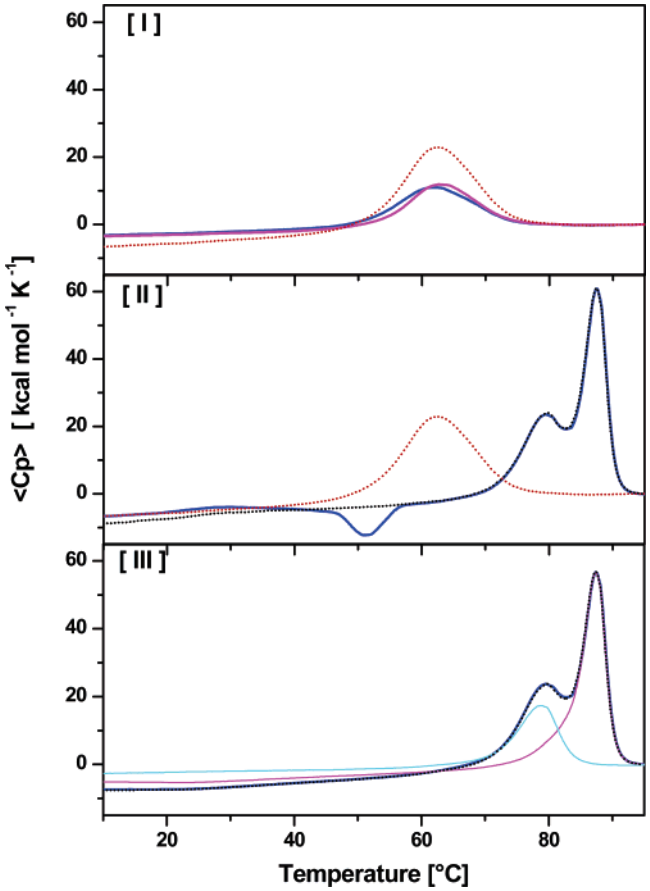

Figure 2. DSC curves of the exchange reaction: (Panel I) Measured excess heat capacity curves of the CTG Ω-DNA (blue) and CAG Ω-DNAs (magenta) in isolation. Also shown is the calculated excess heat capacity curve (red stippled line) that would be expected for a noninteracting 1:1 mixture of the two Ω-DNAs derived by summation of the experimental data. (Panel II) Measured excess heat capacity curves of a 1:1 mixture of CTG Ω-DNA and CAG Ω-DNA upon first heating (blue, solid line). Also shown are the calculated excess heat capacity curves expected for a 1:1 mixture of non-interacting CTG Ω-DNA and CAG Ω-DNA (red, stippled line), and the calculated excess heat capacity curve of a 1:1 mixture of the 22mer and the 40mer duplex (black, stippled curve). Note the exothermic reaction at 50 °C indicative of strand exchange reaction. (Panel III) Excess heat capacity curve of the 1:1 mixture of CTG Ω-DNA and CAG Ω-DNA upon all subsequent heating/cooling scans (blue, solid). For comparison, also shown are the measured excess heat capacity curves of the 22mer duplex (cyan) and the 40mer duplex (magenta), as well as the summed excess heat capacity curves for the 1:1 mixture of the 22mer and 40mer duplex (black, stippled). Note the absence of an exothermic reaction after the first heating scan. To facilitate comparisons the excess apparent heat capacity for all curves is set equal at 95 °C.

denatured state. We therefore conclude that the Ω-DNA-to-duplex transition represents an order−order reaction between metastable states containing unpaired bases in their loops and stable states with all bases fully paired and stacked. We suggest that the strand exchange reaction initiates through interactions of the complementary loop bases, although other possible pathways exist. Indirect support for a role for loop/loop interactions (kissing loops)[57,58] comes from the observation that the strand-swapping reaction happens at lower temperatures when the Ω-DNA concentrations are increased, despite the fact that the isolated bimolecular Ω-DNA bulge loop constructs are individually thermally stabilized by increased DNA concentrations.[54]

Thermodynamic Characterization of the States. Table 2 lists the thermodynamic data we have measured for the conformational transitions along the path from coexisting bulge loop Ω-DNA constructs to the formation of the 22mer and 40mer duplexes, and ultimately to the final single-stranded states. The Supporting Information contains a flowchart that summarizes the relevant thermodynamic data from Table 2 for the strand exchange transformations.

The thermally induced exothermic transition leading to the synchronous formation of the 22mer and 40mer duplexes from the coexisting Ω-DNA constructs is important to our understanding of these metastable intermediates. This reaction is irreversible, only being observed in the first heating curve. For this reason, neither entropy nor free energy can rigorously be determined from the DSC curves, and the temperature at the heat capacity minimum does not have the conventional meaning of a T_m. Nevertheless, our experimental spectral and excess heat capacity curves are correctly described by summation of the relevant experimental data for the isolated Ω-DNA constructs at all temperatures below the onset of the exchange reaction, despite significant differences in experimental time scales (DSC heating at 1 °C/min, UV heating at 0.1 °C/min, CD at 1 spectrum/30 min). Preliminary kinetic experiments (not shown)

(57) Marino, J. P.; Gregorian, R. S., Jr.; Csankovszki, G.; Crothers, D. M. *Science* **1995**, *268*, 1448−1454.
(58) Theilleux-Delalande, V.; Girard, F.; Huynh-Dinh, T.; Lancelot, G.; Paoletti, J. *Eur. J. Biochem.* **2000**, *267*, 2711−2719.

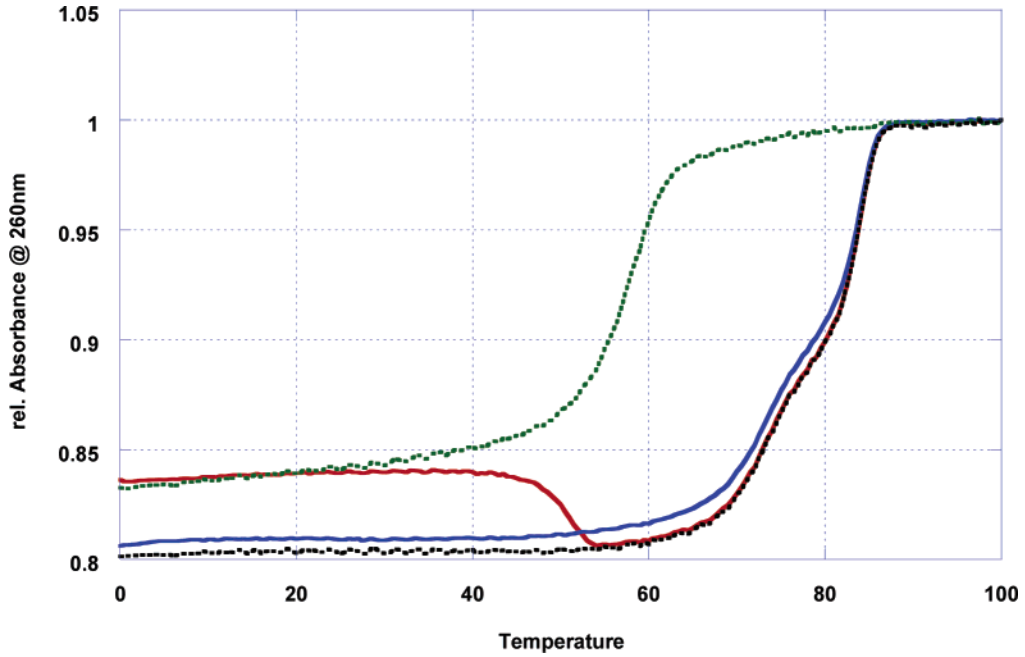

Figure 3. UV melting curves. Comparison of the expected melting curves with the measured temperature-dependent UV melting curves for a 1:1 mixture of CAG Ω-DNA and CTG Ω-DNA. Note the irreversible hypochromic change in the first heating curve (red) compared to the second heating curve (blue). The stippled lines correspond to the expected melting curves for two noninteracting Ω-DNAs (green), and noninteracting 22mer and 40mer duplexes (black).

Table 2. Thermodynamic Data of Ω-DNAs

name	T_m (°C)	ΔH_{cal} (kcal/mol)[a]	ΔS_{cal} (cal/mol/K)	ΔC_{pcal} (cal/mol/K)[b]	$\Delta G_{cal}^{(25\,°C)}$ (kcal/mol)[c]
$X(CAG)_6Y{\cdot}Y'X'$	62.3 ± 0.25	174.5 ± 1.73	520.2 ± 5.63	1083 ± 115.9	17.0 ± 0.3
$Y'(CTG)_6X'{\cdot}XY$	61.4 ± 0.30	177.7 ± 2.66	531.3 ± 8.11	819 ± 157.7	17.6 ± 0.5
$XY{\cdot}Y'X'$	78.4 ± 0.16	160.7 ± 2.02	457.1 ± 5.62	442 ± 88.5	22.5± 0.3
$Y'(CTG)_6X'{\cdot}X(CAG)_6Y$	87.2 ± 0.15	335.1 ± 3.35	930.1 ± 9.7	1132 ± 173.5	51.3 ± 1.0
$X(CAG)_6Y{\cdot}Y'X'$ and $Y'(CTG)_6X'{\cdot}XY$	51.02 ± 0.3	−73.5 ± 5.0 (exchange)	ND	ND	ND
	87.35 ± 0.3	505.7 ± 25.3 (duplex)	1402.7 ± 70.1 (duplex)	ND	87.5 ± 1.8 (duplex)
	87.35 ± 0.3	430.2 ± 30.0 (total)	1193.3 ± 60.0 (total)	ND	74.4 ± 1.5 (total)

[a] 1 cal = 4.184 J. [b] Because of the shape of the heat capacity curve due to the exothermic transition, ΔC_p cannot be reliably determined for the exchange reaction [c] The ΔH, ΔS, and ΔG values correspond to the mean and standard deviation of at least five independent measurements. The reported uncertainties for ΔG likely underestimate the real errors because of statistical linkage between the enthalpy, entropy, and ΔC_p values derived from the same data set.

demonstrate that the exchange reaction only proceeds to a significant extent at elevated temperatures. Consequently, the integrated excess heat capacity curve accurately reflects the heat liberated during the conversion from the two coexisting, noninteracting Ω-DNA complexes to the two Watson−Crick duplexes. As a result we can extract meaningful enthalpy values for this transformation from the measured excess heat capacity curves.

The observation that the exchange reaction is exothermic can be understood in terms of the difference in the nature of the two Ω-DNA constructs relative to the two resulting duplexes. The two duplexes together consist of more Watson−Crick base pairs than the initial two Ω-DNA constructs, whose 18-base bulge loops only become fully base paired and stacked within the center of the 40mer duplex upon strand exchange. The DSC-measured enthalpy required to denature the two newly formed duplexes (Table 2) coincides impressively with the sum of enthalpies measured independently for the 22mer and 40mer duplexes. The enthalpies of denaturation for each of the two Ω-DNA constructs in isolation also have been measured, and are listed in Table 2. These independently measured enthalpy values allow us to calculate (from the heat capacity adjusted differences in enthalpy for the two duplexes and the two isolated Ω-DNAs) a "theoretical" value for the heat released when forming the two duplexes from the two Ω-DNA constructs. Comparison of the calculated value to the measured exothermic enthalpy reveals the experimental exchange enthalpy to be significantly smaller than predicted, even when taking heat capacity changes into account.[59−61] We propose that this disparity between calculated and measured exchange enthalpy reflects the fact that the loop bases are not disordered at the exchange temperature, as is assumed in the calculation of the "theoretical" value. Consequently, part of the enthalpy required for duplex formation from Ω-DNA bulge loop structures already is stored in the order existing in the Ω-DNA constructs at lower temperatures. Support for this interpretation comes from observations that the heat of formation of simple oligonucleotide duplexes at low temperatures, as measured by ITC, does not correspond to the denaturation enthalpy detected by DSC due to considerable single-stranded order at low temperature that poises these singled-stranded structures for duplex formation.[62]

(59) Chalikian, T. V.; Völker, J.; Plum, G. E.; Breslauer, K. J. *Proc. Natl. Acad. Sci. U.S.A.* **1999**, *96*, 7853−7858.
(60) Rouzina, I.; Bloomfield, V. A. *Biophys. J* **1999**, *77*, 3252−3255.
(61) Rouzina, I.; Bloomfield, V. A. *Biophys. J.* **1999**, *77*, 3242−3251.
(62) Vesnaver, G.; Breslauer, K. J. *Proc. Natl. Acad. Sci. U.S.A.* **1991**, *88*, 3569−3573.

Further support for this interpretation comes from our measured excess heat capacity curves and CD spectra on the two 40mer single strands [X(CAG)$_6$Y and Y′(CTG)$_6$X′] which reflect the presence of complex secondary structural elements, consistent with previous reports on single-strand oligonucleotides containing triplet repeat sequences.[63−68]

Strand Displacement in an Ω-DNA Complex by a Complementary Single Strand. We also have investigated the interaction of each of the two Ω- DNA complexes with single strands complementary to either the long (40mer) or the short (22mer) strand involved in the bulge loop structure. As outlined in Scheme 3, a total of four different single-strand/Ω-DNA combinations are possible. Using a combination of CD spectroscopy and differential scanning calorimetry, we have dissected and analyzed how all four possible single strands impact the stability of their respective Ω-DNA partners. We illustrate this experimental approach for the data collected when a 1:1 mixture of the CAG Ω-DNA bulge loop construct is challenged with the Y′(CTG)$_6$X′ single strand (Figures 4 and 5). Comparable results are obtained for the corresponding other three reactions, and are presented in the Supporting Information. The resulting thermodynamic data for all four strand displacement reactions are listed in Table 3. The Supporting Information contains a flowchart that summarizes the relevant thermodynamic data from Table 3 for all the strand displacement transformations.

Thermally Induced, Irreversible Strand Displacement. Our results reveal that addition of either the complementary 22mer single strand or the complementary 40mer single strand to the respective preformed Ω-DNA bulge loop duplex results in the irreversible displacement of one of the strands *only* after the solution is heated above a specific "displacement" temperature. The strand displacement reaction irreversibly results in formation of the thermodynamically more stable, fully paired duplex state plus a released single strand. Below the strand invasion/displacement temperature, the single strand and the corresponding Ω-DNA construct stably coexist.

Spectroscopic and Calorimetric Evidence in Support of Strand Displacement. CD Spectra. Evidence for strand displacement comes from the CD spectra of the 1:1 mixture of the CAG Ω-DNA duplex and the Y′(CTG)$_6$X′ single strand. Upon heating and cooling, the CD spectrum undergoes a significant change from a spectrum that initially is well described by the sum of the CD spectra of the isolated CAG Ω-DNA duplex and the isolated Y′(CTG)$_6$X′ single strand. After heating, the CD spectrum only can be modeled by the sum of the CD spectra corresponding to the 40mer Watson−Crick fully paired duplex and the 22mer Y′X′ single strand, the two products of strand displacement **(**Figure 4, Panels II and III**)**.

DSC and Optical Melting Profiles. The thermally induced change in the CD spectrum is accompanied by an exothermic transition in the excess heat capacity curve, consistent with the formation of a more ordered structure **(**Figure 5, Panel II**)**, as well as a corresponding hypochromic shift in optical melting curves (not shown). The optical changes coupled with the exothermic transition in the DSC curves are seen when either Ω-DNA complex is mixed with its corresponding complementary 40mer single strand. By contrast, when either Ω-DNA is combined with its corresponding complementary 22mer single strand, changes in the CD spectrum are more subtle, and the excess heat capacity curves only show a small positive (endothermic) peak at intermediate temperatures. Nevertheless, comparisons of the melting transition at high temperature with those expected for either the Ω-DNA or the 22mer confirm that the exchange reaction, in fact, has occurred, despite the relative absence of the optical and calorimetric signatures noted for the strand displacement process involving the 40mer.

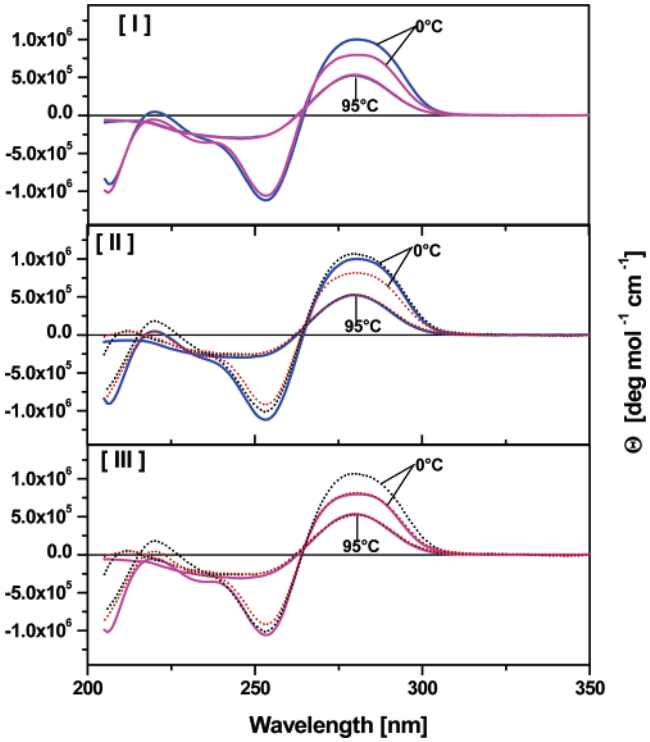

Figure 4. CD curves Y′(CTG)$_6$X′ 40mer and CAG Ω-DNA. (Panel I) Experimentally measured CD spectra of a 1:1 mixture of CAG Ω-DNA and the Y′(CTG)$_6$X′ 40mer strand at 0 °C prior to heating (blue, solid) and after heating to 95 °C and cooling (magenta, solid). Also shown as internal controls, are the CD spectra at 95 °C (solid, blue and magenta). (Panel II) Comparison of the measured spectrum (blue solid) prior to heating to the CD spectra calculated for a 1:1 mixture of the CAG Ω-DNA and Y′(CTG)$_6$X′ 40mer strand (black stippled line) and for the 1:1 mixture of the 40 mer duplex and Y′X′ 22mer (red stippled line). (Panel III) Comparison of the corresponding experimental CD spectrum after heating (magenta, solid) to the calculated spectra, as in (Panel II). Also shown as internal controls in Panels II and III are the calculated (red and black stippled line) and measured (blue and magenta solid) CD spectra at 95 °C. Calculated spectra are derived by summation of experimentally measured spectra of the isolated individual components. The corresponding CD spectra for the other strand displacement reactions are shown in the Supporting Information.

To summarize, the strand displacement reaction for the 40 + 22 Ω-DNA plus complementary 40mer is exothermic and irreversible, whereas the strand displacement reaction for the 22mers is endothermic and irreversible. We propose that the endothermic excess enthalpy for the 40 + 22 Ω-DNA plus 22mer strand displacement derives from contributions of the unfolding of some secondary structure in the loop domain of the Ω-DNA which, upon cooling, is recovered through folding of the displaced single strand 40mer, as discussed below. The differences in the CD spectra, as well as the excess heat capacity

(63) Amrane, S.; Sacca, B.; Mills, M.; Chauhan, M.; Klump, H. H.; Mergny, J.-L. *Nucleic Acids Res.* **2005**, *33*, 4065−4077.
(64) Gacy, A. M.; Goellner, G.; Juranic, N.; Macura, S.; McMurray, C. T. *Cell* **1995**, *81*, 533−540.
(65) Gacy, A. M.; McMurray, C. T. *Biochemistry* **1998**, *37*, 9426−9434.
(66) Paiva, A. M.; Sheardy, R. D. *Biochemistry* **2004**, *43*, 14218−14227.
(67) Petruska, J.; Arnheim, N.; Goodman, M. F. *Nucleic Acids Res.* **1996**, *24*, 1992−1998.
(68) Petruska, J.; Hartenstine, M. J.; Goodman, M. F. *J. Biol. Chem.* **1998**, *273*, 5204−5210.

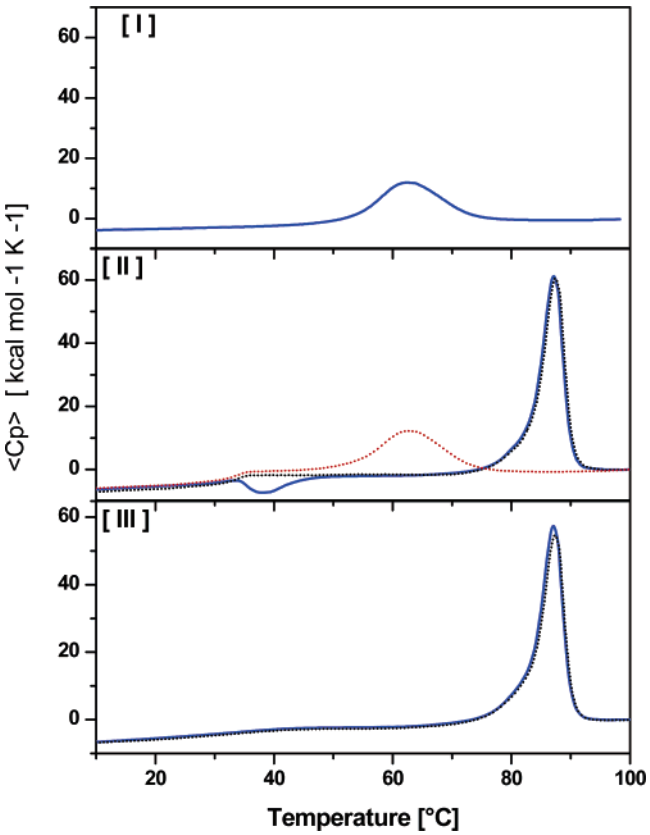

Figure 5. DSC curves Y′(CTG)$_6$X′ 40mer and CAG Ω-DNA. (Panel I) Measured excess heat capacity curves of the CAG Ω-DNAs (blue, solid) in isolation. (Panel II) Measured excess heat capacity curve of a 1:1 mixture of the Y′(CTG)$_6$X′ 40mer and CAG Ω-DNA upon first heating (blue, solid line). Also shown are the calculated excess heat capacity curves of a 1:1 mixture of the Y′(CTG)$_6$X′ 40mer and CAG Ω-DNA (red, stippled line) as well as the calculated excess heat capacity curve of a 1:1 mixture of the Y′(CTG)$_6$X′ 40mer single strand and the 40mer duplex (black, stippled line). Note the exothermic reaction near 40 °C, indicative of the strand displacement reaction. (Panel III) Excess heat capacity curve of the 1:1 mixture of the CTG 40mer single strand and CAG Ω-DNA (blue solid) upon all subsequent heating events. For comparison, the calculated excess heat capacity curves of the Y′X′ 22mer single strand and the 40mer duplex are shown (black stippled). Note the absence of an exothermic reaction in all scans after the first heating scan. To facilitate comparison, the excess apparent heat capacity for all curves is set equal at 95 °C. The corresponding DSC curves for the other strand displacement reactions are shown in the Supporting Information.

curves, reflect the net change in the number of base pairs associated with a given strand displacement reaction. Note that the change from Ω-DNA complex to 22mer duplex results in no net change in the total number of base pairs, whereas the change from Ω-DNA complex to 40mer duplex increases the total number of base pairs by 18.

The strand displacement in the Ω-DNA complex by the corresponding 22mer single strand occurs near 50 °C for both sets of Ω-DNA complexes, whereas strand displacement between Ω-DNA and the complementary 40mer single strand occurs at significantly lower temperature (about 40 °C). Both Ω-DNA complexes, on their own, begin to melt near 50 °C. These observations suggest that Ω-DNA structure needs to be partially disrupted before the added 22mer can successfully displace the 40mer strand from the Ω-DNA secondary structure. By contrast, the 40mer requires no partial disruption of the Ω-DNA structure to initiate displacement of the 22mer and to form the duplex.

Single-Stranded Order Modulates the Energetics of Strand Displacement. Inspection of the excess heat capacity curves reveals that the single-stranded secondary structure of the incoming 40mer needs to denature partially before the strand displacement reaction initiates. These results are consistent with the assumption that the partially unfolded 40mer initiates strand displacement through loop/single strand interactions. The observation that the long, 40mer single strand has to be partially unfolded prior to interacting with its complementary Ω-DNA whereas the short, 22mer single strand requires partial disruption of the Ω-DNA prior to interacting with it is of relevance to the pathway of strand exchange between the complementary Ω-DNA complexes discussed above.

Conceptually, one can rationalize the exothermic transition observed when a 40mer single strand interacts with an Ω-DNA construct in terms of the formation of an additional 18 base pairs in the center of the newly formed 40mer helix. By contrast, the displacement reaction between the short 22mer and the Ω-DNA does not result in a net change in the total number of base pairs. In addition to disrupting the Ω-DNA structure and forming a new duplex, the strand displacement reaction removes one single strand to form the duplex and liberates a second single strand from the Ω-DNA. Inspection of the excess heat capacity curves measured for each of the single strands reveals that most of the single strands undergo a melting transition in the temperature range where the strand displacement reaction takes place. Formation of the newly formed duplex from the Ω-DNA is therefore associated with disruption of the residual secondary structure of the incoming single strand and formation of partial new secondary structure in the leaving strand. This interpretation is supported by the close agreement between the summed excess heat capacity curves for the incoming single strand plus Ω-DNA construct prior to the onset of the displacement reaction, as well as the close agreement of the summed heat capacity curves of the newly released single strand plus duplex after completion of the displacement reaction (Figure 5, Panel II).

In the case of the CAG Ω-DNA construct plus 22mer single strand, the DSC curves reveal that the incoming 22mer single strand exhibits no secondary structure and the leaving 40mer strand is mostly denatured at the displacement temperature (T = 51 °C). Consequently, for this displacement reaction, we find that the heat of denaturation of the CAG Ω-DNA subtracted from the heat of denaturation of the 22mer duplex (taking ΔC_p into account)[59−61] correctly predicts the measured endothermic heat for the displacement reaction ($\Delta\Delta H$ = 12 kcal/mol). For the other reactions, however, we find that the calculated displacement heat exceeds the measured heat. This observation is consistent with such additive calculations not always correctly accounting for the contributions of the single strands. In fact, the enthalpies determined for the melting of the isolated single strands may not exclusively reflect the melting of secondary structure in the same single strands in the context of the Ω-DNA during the displacement reaction. In other words, this observation informs our interpretation of the molecular origins of the exchange enthalpy for the Ω-DNA /Ω-DNA exchange reaction discussed above.

Biological Implications. We have demonstrated that metastable DNA secondary structures can stably coexist in solution below a critical temperature, trapped in kinetically protected states. In other words, energy landscapes for nucleic acid folding

Table 3. Thermodynamic Data for Single Strand Displacement

name	reaction	T_m (°C)	ΔH_{cal} (kcal/mol)	ΔS_{cal} (cal/mol/K)	ΔC_{pcal} (cal/mol/K)[a]
		Exchange Long Strand			
$X(CAG)_6Y{\cdot}Y'X' + Y'(CTG)_6X'$	Ω CAG	62.1	174.9 ± 8.7	521.7 ± 26.0	1190 ± 238
	exchange	39.2	−26.5 ± 2.6	N/D	N/D
		87.1	332.1 ± 16.6	921.9 ± 46.1	N/D
	rescan	87.1	337.2 ± 16.9	936.0 ± 46.8	960 ± 192
$Y'(CTG)_6X'{\cdot}XY + X(CAG)_6Y$	Ω CTG	61.4	180.7 ± 9.0	540.1 ± 27.0	746 ± 149
	exchange	39.9	−39.5 ± 3.9	N/D	N/D
		87.2	331.4 ± 16.6	919.7 ± 46.0	N/D
	rescan	87.1	335.4 ± 16.8	929.9 ± 46.5	1130 ± 226
		Exchange Short Strand			
$X(CAG)_6Y{\cdot}Y'X' + XY$	Ω CAG	62.3	176.0 ± 8.8	524.6 ± 26.2	1100± 220
	exchange	51.0	12.1 ± 1.3	N/D	N/D
		78.3	160.0 ± 8.0	455.2 ± 22.8	N/D
	rescan	78.4	163.1 ± 8.1	463.9 ± 23.2	N/D
$Y'(CTG)_6X'{\cdot}XY + Y'X'$	Ω CTG	61.1	177.1 ± 8.8	529.8 ± 26.5	1000 ± 200
	exchange	47.6	58.3 ± 5.8	N/D	N/D
		78.3	160.0 ± 8.0	455.2 ± 22.8	N/D
	rescan	78.4	158.1 ± 7.9	449.7 ± 22.5	N/D

[a] Because of the shape of the heat capacity curve due to the single-stranded (added or exchanged) contributions, ΔC_p cannot be reliably determined for all displacement reactions.

pathways may contain local minima, with significant activation barriers between metastable states and the global energy minimum.[69−71] This recognition supports models of DNA function that require transient population of thermodynamically unfavorable states as part of the overall process, such as those invoked to explain DNA expansion/contraction and/or chromosome instability.[15,16,31,34,35,37,38,47,72,73] DNA strand separation during transcription and translation, and/or the formation of single-strand domains during DNA repair in highly repetitive sequences can lead to the transient formation of metastable bulge loops/slipped DNA states in vivo, that share similarities to the model systems reported here. In fact, the influences of negative supercoiling, more extended duplex domains (e.g., the absence of free ends), and protein binding may further stabilize such metastable intermediates in vivo. Our results suggest that, once formed, metastable, bulge loop DNA structures can persist, perhaps ultimately contributing to DNA expansion/deletions, thereby supporting in vivo models that invoke important biological roles for local minima within DNA energy landscapes.

Conclusion

We have described the strand exchange behavior of two 40mer bulge loop Ω-DNA constructs when challenged with each other, as well as their strand displacement reactions when challenged with either a fully complementary 40mer sequence, or a partially complementary 22mer single strand. Our data reveal that metastable, bulge loop states can be highly populated at physiological temperatures, consistent with such conformational forms being biologically relevant in vivo, as has been proposed in a range of disease and/or mutation-inducing mechanisms. In short, our results reveal the nucleic acid energy landscape available to biological processes to be more complex than conventionally assumed on the basis of traditional investigations of helix-to-coil transitions. Such studies enhance our understanding of the formation and relative stability of transient nucleic acid intermediates of potential biological significance.

Acknowledgment. We thank Dr. G. Eric Plum (Ibet Inc. and Rutgers University) for many helpful discussions. This work was supported by National Institutes of Health Grants GM23509, GM34469, and CA47995 (to K.J.B.).

Supporting Information Available: Flowcharts summarizing the thermodynamics of strand exchange and strand displacement; CD spectra and DSC thermograms for three strand displacement reactions not shown in the main text. This material is available free of charge via the Internet at http://pubs.acs.org.

JA070258Q

(69) Frauenfelder, H. *J. Biol. Phys.* **2005**, *31*, 413−416.
(70) Thirumalai, D.; Hyeon, C. *Biochemistry* **2005**, *44*, 4957−4970.
(71) Ansari, A.; Kuznetsov, S. V.; Shen, Y. *Proc. Natl. Acad. Sci. U.S.A.* **2001**, *98*, 7771−7776.
(72) Cleary, J. D.; Pearson, C. E. *Trends Genet.* **2005**, *21*, 272−280.
(73) Richards, R. I. *Trends Genet.* **2001**, *17*, 339−345.